SCUOLA DI INGEGNERIA INDUSTRIALE
E DELL'INFORMAZIONE

Simulation of a LEO orbiting microsat on Simulink

MSc in Space Engineering

Authors:

10723712	Marcello Pareschi	(BSc Aerospace Engineering - Politecnico di Milano)
10836125	Daniele Paternoster	(BSc Aerospace Engineering - Politecnico di Milano)
10711624	Alex Cristian Turcu	(BSc Aerospace Engineering - Politecnico di Milano)
10884250	Tamim Harun Or	(BCs Aerospace Engineering - International Islamic University Malaysia)

Professor: Franco Bernelli Zazzera

Academic year: 2023-2024

Abstract

La presente relazione di prova finale intende dare una descrizione dell'endoreattore F-1 prodotto da Rocketdyne. Cinque di questi motori vennero installati sul primo stadio S-IC del vettore Saturn V che portò il primo uomo sulla luna. L'obiettivo di questo stadio era quello di portare il razzo ad una quota di 61 km, fornendo un $\Delta v \simeq 2300$ m/s. Questo primo requisito verrà mostrato attraverso un modello matematico che simula il volo dello stadio S-IC.
Di seguito verranno analizzati i principali sistemi per un singolo motore, partendo dal sistema di storaggio e alimentazione dei propellenti costituito dai serbatoi e dalla turbopompa, passando per il sistema di generazione di potenza che comprende il gas generator e la turbina. Passando dalla camera di combustione si arriva infine al sistema di espansione gasdinamico e allo studio del suo raffreddamento. Si provvederà inoltre a dare una descrizione qualitativa e quantitativa delle scelte progettuali applicate ai tempi.
La discussione dei processi di combustione del gas generator e della camera di spinta si basa su dati provenienti da simulazioni eseguite con i programmi CEAM e RPA.

Contents

1. Symbols

1.1. Analisi della missione

$\boldsymbol{A_e}$	$[m^2]$	area di efflusso totale
$\boldsymbol{\phi}$	$[rad]$	angolo di traiettoria del razzo

1.2. Analisi della missione 2

$\boldsymbol{A_e}$	$[m^2]$	area di efflusso totale
$\boldsymbol{\phi}$	$[rad]$	angolo di traiettoria del razzo

2. Requirements

2.1. Mandatory requests for simulation

[1]

3. Framework Analysis

3.1. Satellite characterization

The group was inspired by ESAIL, a microsatellite, developed by exactEarth in cooperation with ESA, which has the mission of ship targeting. Two configurations of the satellite were implemented: the undeployed configuration, for the detumbling phase, and the extended configutation, for the slew and tracking phase. The latter was modeled as a cubic central body, of side 70 cm, and four solar panels, modeled as rectangular bodies of dimensions $70 \times 70 \times 1\ cm$. Solar panels are set along y axis of body frame, as shown in figure ,with normal parallel to z axis of body frame.

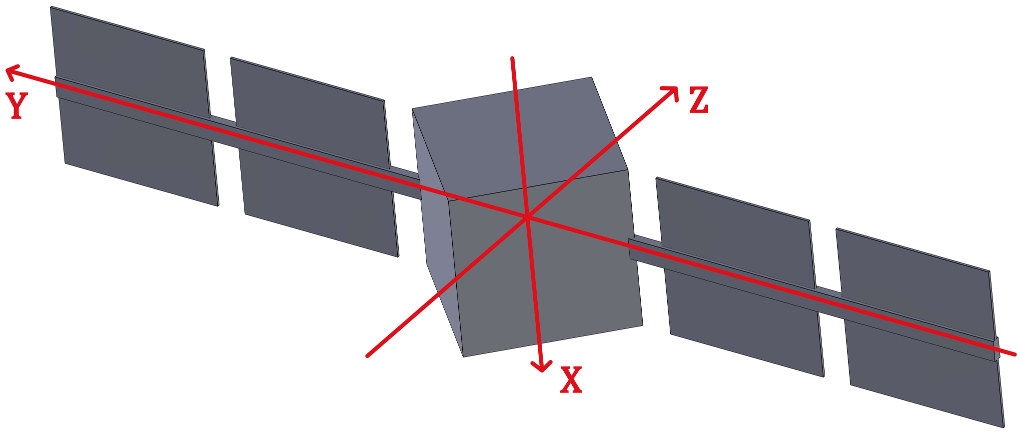

Figure 1: Satellite model

The mass was assumed to be 100 Kg and the satellite was considered to be, in first approximation, isotropic. Under these assumptions, the inertia matrix was computed as

$$I = \begin{bmatrix} 22.9724 & 0 & 0 \\ 0 & 7.7770 & 0 \\ 0 & 0 & 23.1895 \end{bmatrix} Kg\ m^2 \tag{1}$$

On the other hand, the undeployed configuration was implemented as a isotropic cube of side 70 cm, with mass $m = 100\ Kg$ The inertia matrix of the undeployed configuration is then

$$I = \begin{bmatrix} 8.1667 & 0 & 0 \\ 0 & 8.1667 & 0 \\ 0 & 0 & 8.1667 \end{bmatrix} Kg\ m^2 \tag{2}$$

3.2. Orbit characterization

The orbit adopted for the simulation is a Sun-synchronous (SSO), nearly polar and LEO orbit. Polar orbits allows to scan the whole globe during the several orbits, due to Earth rotation. SSO are orbits that maintain the same angle between their orbital plane and the direction that connects the Earth with the Sun [2]. This allows the spacecraft the monitor the Earth surface with always the same conditions of light (or eventually darkness, if the plane is oriented in a certain way). Also, a SSO orbit can be choosen in such a way to have always the sun visible [3].
The real data are based on the ephemeris of the ESAIL mission from which we were inspired. In particular, it was taken the orbital parameters on 16/12/2023 at 12 UT of ESAIL satellite, then we propagated the orbit using the simple two body problem without any perturbation. This clearly is an approximation since several distrubances act on the satellite as it will be seen in section 6, also the SSO orbits are intrisically caused by the J2 effect of Earth. Nevertheless, the simulation of few LEO orbit's periods considered in this report wouldn't be enough to show the

distrubances effects caused on the motion of the centre of mass of the satellite. The advantage to take as initial condition the ephemeris is that the motion of the spacecraft in those two or three periods of the orbit of simulation that are considered is seen as sun-synchronous. Infact, that time of simulation taken into account is a snapshot compared to the time of action of the J2 effect responsible for the SSO orbit, that is one year. Clearly, a more detailed simulation should consider the variation of the orbital parameters due to J2 and all other perturbations.
The orbital parameters chosen, following the description given above, are:

$a\,[km]$	$e\,[-]$	$i\,[\text{deg}]$	$\omega\,[\text{deg}]$	$\Omega\,[\text{deg}]$
6851	0.0018	97.40	101.58	0

Table 1: Orbital Parameters

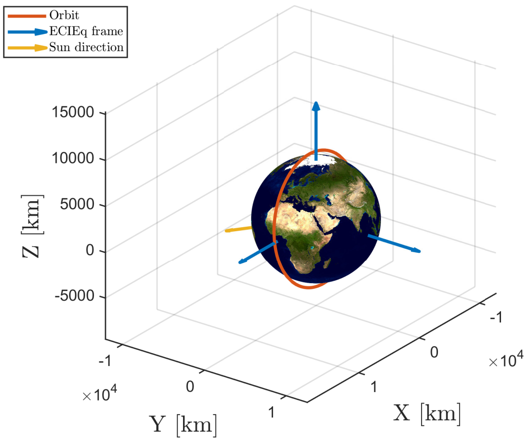

Figure 2: Orbit Representation

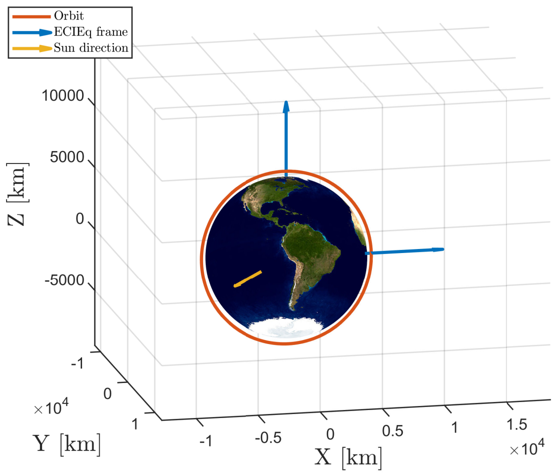

Figure 3: Sun Direction view

In the Figure 2 and Figure 3 the sun direction is also plotted, in this case it is possible to see that the orbit doesn't go into eclipse condition.
On Simulink, the model for the orbital position implemented is based on the integration of the true anomaly

$$\dot{\theta} = \frac{n\,(1 + e\cos\theta)^2}{(1 - e^2)^{3/2}}$$

Then, the radial distance is found as:

$$r = \frac{a\left(1 - e^2\right)}{1 + e\cos\theta}$$

At this point it is easy to retrieve the position $\boldsymbol{r_p}$ of the S/C in the perifocal frame $\mathcal{P}$.

$$\underline{r}_P = r \begin{bmatrix} cos\theta \\ sin\theta \\ 0 \end{bmatrix} \tag{3}$$

.
The position in the inertial frame $\mathcal{N}$ is found using the the transpose of the transformation matrix $\boldsymbol{A_{pn}} = \boldsymbol{R_3}(\omega)\boldsymbol{R_1}(i)\boldsymbol{R_3}(\Omega)$. In particular:

$$\boldsymbol{r_n} = \boldsymbol{A_{pn}} \boldsymbol{r_p}$$

4. Dynamics

The equations of the dynamics rotating body motion used throughout the simulation are the Euler equations since rigid body motion assumption is made. The set of equations are referred to the principal axis frame of the satellite. This frame will be also called reference frame $\mathcal{B}$, it is described by three unit vectors $\{\boldsymbol{x_b}, \boldsymbol{y_b}, \boldsymbol{z_b},\}$, that are in the direction of principal inertia axis.

$$\boldsymbol{I}\,\dot{\boldsymbol{\omega}} + \boldsymbol{\omega} \times \boldsymbol{I}\,\boldsymbol{\omega} = \boldsymbol{M_d} + \boldsymbol{M_c}$$

In the above equation the external torque has been divided in to 2 contributions, with clear distinction. M_d describes the disturbance torques that act on the spacecraft due to environment and presented in the previous section, while M_c is referred to the control torque that the actuators are generating to perform the tasks required by the control logic.
With particular reference to the Simulink model, two configurations of the satellite were considered: undeployed configuration (for detumbling phase) and extended configuration (for slew and pointing phases). As a consequence, the mass distribution and hence the inertia matrix are different in terms of numerical values. This fact has been taken into account by implementing a logic in the dynamic block of Simulink, that switches between the two matrices using a flag based on the activation of the De-Tumbling control. This istantaneous switch is not completely realistic since the extraction of the panels would require some finite time, and in some way could influence the real dynamic of the satellite. Anyhow, for the microsat considered, the retracted configuration allows a faster detumbling, and also inertia loads and stresses are reduced on the solar panels.

5. Kinematics

As specified in section 2, the attitude parameters of the satellite are expressed through the use of Euler angles. The kinematics calculated according to this parameterization follows these steps:

- given the angular velocity ω from dynamics for each time and the initial condition on Euler angles s_0, compute the time derivatives of the angles $\dot{s}$;
- integrate the derivatives to obtain the set of Euler angles s for each time;
- from the calculated angles, compute the attitude matrix A.

The main problem when dealing with this kind of parameterization is that, for any chosen set of three Euler angles, there are always some singularity conditions on the second angle θ that could make the derivatives of the other two angles tend to infinite. The problem is related to the fact that, in this particular conditions, the set of Euler angles is not uniquely defined, since the first and the third rotation are done on the same physical direction.
To avoid these singularities, it becomes necessary to have two systems working on two different sets of Euler angles:

- one set of angles defined by three different indexes, which have the singularity condition on $\theta = (2n+1)\pi/2$;
- one set of angles where the first and the last indexes coincide, which have the singularity condition on $\theta = n\pi$.

To merge these two systems together and avoid all the singularities, there are two main paths:

- run both systems all the time, get the attitude kinematics only from one system until it reaches its singularity condition on θ, then switch to the other system, which will be further from its singularity;
- run just one system at a time; when the system reaches its singularity condition, convert from the current set of angles to the other set through the attitude matrix, impose the calculated angles as the initial condition of the system, then start the integration from where it interrupted, deactivating the system that reached the singularity.

Although the first option is simpler, the second option offers significant computational savings for the simulation. It is important to note that the kinematics model is only executed in the simulation to calculate the satellite's motion over time and is not executed on the satellite processor. Despite the added complexity of the system switch, the second option was chosen to accelerate the execution of the Simulink model.
...

6. Disturbances analysis

In order to make a realistic simulation of the rotating motion of the spacecraft, the environment distrubances has to be taken into account. The preliminary study of these external torques is crucial for a realistic simulation. In the following paragraphs a brief introduction will be done for all the main disturbances, then the simulation of the specific satellite and orbit will be presented, mainly to choose the two most relevant disturbances. This choice is reasonable since there are always two predominant effects of disturbance, while the other can be supposed small (usually some order of magnitude smaller, but always depends on the specific case).

6.1. Magnetic Disturbance

The influence of the Earth's magnetic field on the satellite is relevant due to the proximity of the orbit taken in exam. Besides the crucial role that it plays in the actuation, the magnetic field could also cause big disturbances on the satellite's dynamics. The magnetic torque, whether generated by the magnetorquers or by parasitic currents present in the satellite, follows the general law:

$$\boldsymbol{M} = \boldsymbol{D} \wedge \boldsymbol{B}$$

where $\boldsymbol{D}$ is the magnetic dipole generated by a coil or by parasitic currents, $\boldsymbol{B}$ is the magnetic field vector.

A mathematical model of the magnetic field is necessary to evaluate $\boldsymbol{B}$ given the satellite position along the orbit. The model chosen for the purpose is the 13th edition of the International Geomagnetic Reference Field (IGRF). According to this model, the magnetic field $\boldsymbol{B}$ is evaluated as the gradient of a magnetic scalar potential V, which is modelled as a spherical harmonic expansion of order N:

$$\boldsymbol{B}(r,\theta,\phi,t) = -\nabla V(r,\theta,\phi,t) \qquad V(r,\theta,\phi,t) = a\sum_{n=1}^{N}\sum_{m=0}^{n}\left(\frac{a}{r}\right)^{n+1}\left(g^{n,m}(t)\cos m\phi + h^{n,m}(t)\sin m\phi\right)P^{n,m}(\cos\theta)$$

where r,θ,ϕ are the spherical coordinates of the satellite in a Earth-Centered Earth-Fixed (ECEF) frame, a is the Earth's equatorial radius (6371.2 km), $P^{n,m}(\cos\theta)$ are the Gauss normalized associated Legendre functions, $g^{n,m}(t)$ and $h^{n,m}(t)$ are the Schmidt semi-normalized spherical harmonic coefficients. These coefficients are computed from experimental data and depend on time, as the Earth magnetic field is not constant but changes significantly every year. In this simulation, the coefficients refer to year 2020 of IGRF-13 and the expansion is computed up to order 13. Note that the model must be in the ECEF frame because the magnetic field rotates with the Earth. To adapt the model to an Earth-Centered Inertial (ECI) frame, a rotation matrix is required for the input and its transpose for the output. The matrix takes account of the angular velocity of the planet on time. Lastly, the magnetic field $\boldsymbol{B}$ can be expressed in the body frame through the attitude matrix.
Once that $\boldsymbol{B}$ is defined for every satellite position, the $\boldsymbol{D}$ vector is chosen as an arbitrary constant (based on typical microsat values) and the torque is easily computed along the orbit thanks to the previous formula.

6.2. SRP Disturbance

SRP radiation torque is the disturbance generated by electromagnetic waves that impacts on the spacecraft panels and generate a force. These forces acting on some of the panels could give rise to a net torque around the center of mass of the spacecraft. Only sun radiation will be considered in this case, a more deep analysis should consider infrared Earth radiation and reflected Earth radiation. In addition, no eclipse condition will be analyzed during all the simulation, a reasonable assumption for the sun-synchronous case orbit.
The formula to calculate the force acting on each discrete panel is:

$$\boldsymbol{F_i} = -PA_i\left(\hat{S}_B\cdot\hat{N}_{B,i}\right)\left[(1-\rho_s)\hat{S}_B + \left(2\rho_s\left(\hat{S}_B\cdot\hat{N}_{B,i}\right) + \frac{2}{3}\rho_d\right)\hat{N}_{B,i}\right]$$

In order to simulate this kind of disturbance the coefficients of absorption, specular reflection and diffusion has to be decided. These values clearly depends on the material that will be choosen to construct the main body of the spacecraft, and the solar panels. Since these parameters are related through an energetic balance, we could only decide two of them and the third follows. In order to determine the force on each surface, also the geometry of the panels of the satellite has to be given, in particular size of each panel(fully defined in section ...) and direction of the normal of the panel in $\mathcal{B}$ frame. The direction of sun $\hat{S}_B$, has been firstly modeled in ECI frame considering the obliquity ϵ of earth's rotation axis with respect to the ecliptic plane, then through attitude matrix, the unit vector $\hat{S}_B$ has been computed. Lastly, to caluclate the torque we should known where the resulting force on each panel acts (i.e. the centre of SRP force for each panel). No detailed calulation has been made on this aspect, it is assumed as first approximation that the forces acts on the geometric center of the corresponding plate. Also, in order to correctly calculate the total torque a shadow check must be performed, this is simply implementated in Simulink by checkin the sign of the dot product of the normal versor of the plate and the sun direction.

6.3. Drag Disturbance

Over extended periods, the spacecraft's engagement with the higher strates of Earth's atmosphere results in the generation of a torque around its mass center. This influence may not be trivial. At altitudes less than 400 kilometers, the aerodynamic torque is the predominant factor, though its significance diminishes considerably beyond 700 kilometers altitude. For the simulation, the panels are considered from geometry data of section (..ref) the coefficient of drag C_d has been set to 2.2, the relative velocity consideres the rotation of Earth around its axis and also the rotation motion of the spacecraft. As for the SRP case, a sort of shadow check has to be implemented based on the dot product between the relative velocity and the normal of the surface. This check is required since the modelling of the surface is composed of two faces, usually one impacts with the relative air movement while the other is behind and doesn't impact. As for SRP disturbance, for the drag torque the vector r_i as distance of centre of pressure to centre of mass, should be evaluated. As a first approximation, the point of action of the force for each face is the middle point of the surface under consideration.

$$T_{AERO} = \begin{cases} \sum_{i=1}^{n} \vec{r}_i \times \vec{F}_i, & \text{if } \vec{N}_{bi}\cdot\vec{v}^{b}_{rel} \geq 0 \\ 0, & \text{if } \vec{N}_{bi}\cdot\vec{v}^{b}_{rel} < 0 \end{cases} \quad \text{with}$$

$$\vec{F}_i = -\frac{1}{2}\rho C_D v_{rel}^2 \vec{v}^{b}_{rel}(\vec{N}_{bi}\cdot\vec{v}^{b}_{rel})A_i \quad \text{n=number of faces}$$

6.4. Gravity Gradient Disturbance

The gravity gradient disturbance account for the fact that the gravity around the spacecraft is not uniform, hence a non-negligible torque will arise from there. Studying the torque generated by an elementary force acting on the elementary mass dm the equation for this is obtained:

$$dM = -\mathbf{r} \times \frac{Gm_t dm}{|\mathbf{R}+\mathbf{r}|^3}(\mathbf{R}+\mathbf{r})$$

Where $\mathbf{r}$ is the distance of dm from the centre of mass and $\mathbf{R}$ is the distance of the centre of mass from the centre of the Earth. Approximating this equation, and expressing the position vector of the centre of mass as the product of magnitude (R) with the direction cosines, it's possible to centre this torque in the principal inertia axes. Integrating this equation the final form is achieved.

$$M_x = \frac{3Gm_t}{R^3}(I_z - I_y)c_2c_3$$
$$M_y = \frac{3Gm_t}{R^3}(I_x - I_z)c_1c_3$$
$$M_z = \frac{3Gm_t}{R^3}(I_y - I_x)c_1c_2$$

The c_1, c_2 and c_3 are the direction cosines of the radial direction in the principal axes. Therefore if one of the principal axes is aligned with the radial direction the torque will be zero because only one of the direction cosines is non-zero. It's clear that this disturbance acts in a continuous manner throughout the orbit motion and the torque produced depends mainly on the attitude matrix.
Instead, the stability configuration depends on the distribution of mass of the spacecraft with respect to the orientation we want to achieve. For our case of study, inspired by the ESAIL mission from ESA, the satellite is nadir pointing. In particular the $\boldsymbol{x_b}$ direction has to be aligned with the nadir, while the $\boldsymbol{z_b}$ has to point the sun for solar panels requirements. Using the numerical values of the spacecraft, and the orientation requriements just mentioned this particular configuration results unstable to GG disturbance.

6.5. Simulation of all disturbances

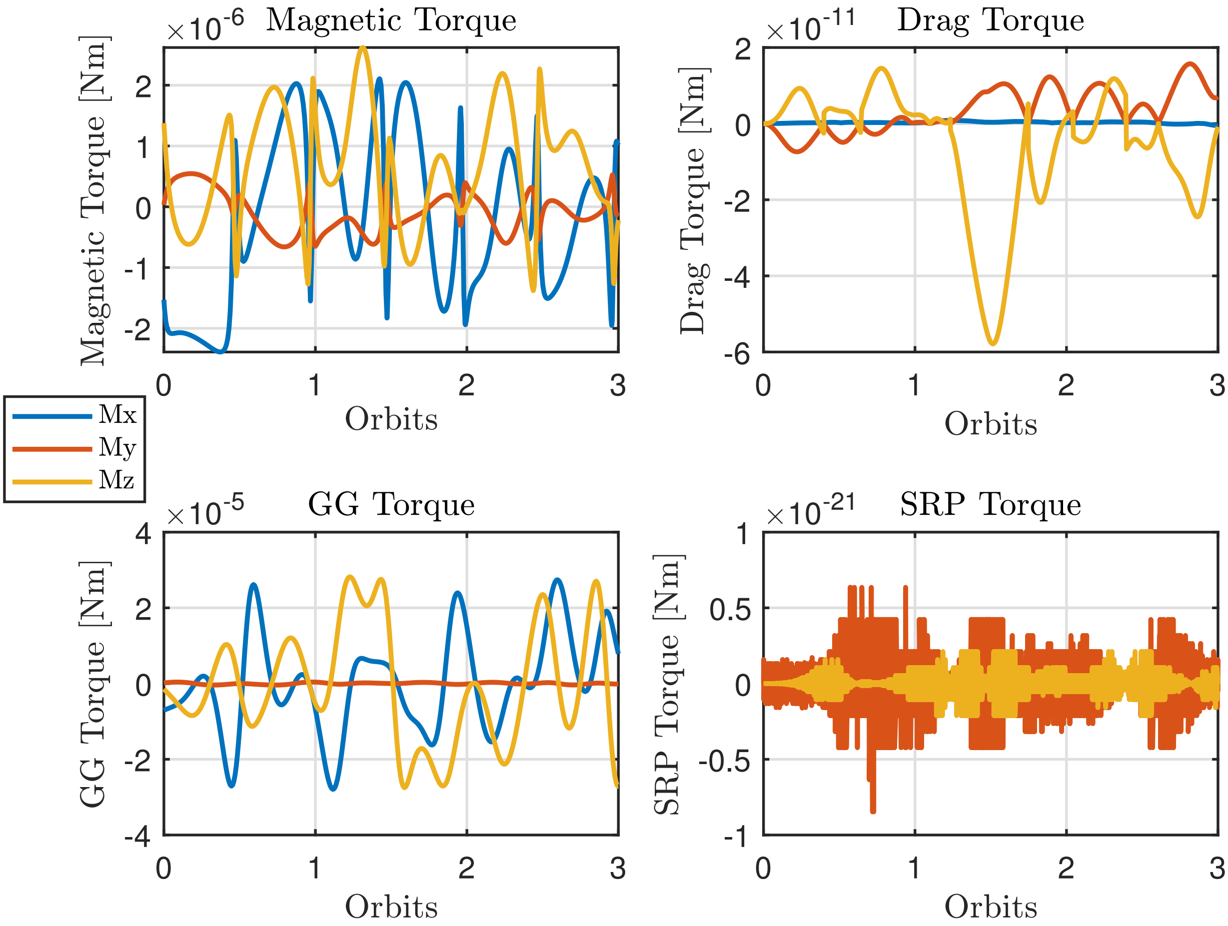

Figure 4: Simulation of all disturbances

The control-free motion has been simulated with all the disturbances for three full periods. The initial condition were set to null initial angular velocity and null Euler angles in the 312 set.
From the graphs of Figure 4 it is clear that SRP disturbance is negligible in our case, the graph shows only numerical zeros. In particular, this is due to the simmetry of the geometry of the spacecraft a small set off for the CoM would have produced a net torque. It is clear, that in this specific case, the two most relevant disturbances are due to magnetic field interaction and the gravity gradient torque since the atmospehric drag torque is some orders of magnitude smaller.
Note that in the Gravity Gradient torque the y-axis component is almost null compared to the other components along x and z, this is due to the fact that the y-axis component of the torque depends on the difference between inertia moment along x and along z, for our case those two moments of inertia are very similar (reference).

7. Sensors

Sensors are fundamental tools that allows the SC to know its orientation or angular velocity. Their presence onboard is fundamental for having a controlled motion of the satellite. In this section, the 3 sensors used will be presented, it will be also clarified the motivation that lead the team to choose two additional sensors over the horizon sensor assigned.

7.1. Horizon Sensor

Horizon sensors are devices that can detect the centre of the planet, in our case Earth, and reconstruct the direction of that point with respect to the satellite. They usually work by analyzing the IR spectrum of the image through a thermopile to reduce the visible light spectrum interference caused by transition of day and night on earth. Due to the nadir pointing requirment a static earth sensor has been chosen for this specific application. In particular, the

Meisei Earth Horizon was chosen, which has the following specifics:

$F.O.V.$ [deg]	$Accuracy$ [deg]	$Frequency\,[Hz]$
33	1	30

Table 2: Real data for Horizon Sensor

Due to operational requirements, the static sensor has to point the Earth, in particular the optical axis must have the same direction of the nadir (direction that links centre of earth and CoM of the S/C). To fulfill this request, a good option could be to position the sensor on the face that also contains the payload, that is the face of the spacecraft main body (cube) that has normal along the $\boldsymbol{x_b}$ direction.
The model implemented to simulate the behaviour of the sensor in the Simulink environment takes the real position of the S/C with respect to centre of Earth expressed in inertial space, changes its direction multiplying by -1 and expresses it in the $\mathcal{B}$ frame through the real attitude matrix $\boldsymbol{A_{B,N}}$. This unit vector is the input of the sensor block, here it is sampled through a zero-order hold of frequency specified by Table 2 to simulate the digital nature of the sensor. Then some errors of measurments has to be added. It was decided to model two typical effects of real sensor: the mounting error that cause misalignment and also an accuracy error modeled with a band-limited white noise on all the components of the direction vector. Chronologically, first the misalignment is calculated, then the noise is introduced:

- The misalignment error was computed on Simulink by introducing a small deviation with respect to the nominal condition. This can be done by adding a small-scaled vector in the direction perpendicular of the unit vector that has to be measured. The scaling of this vector has to be small with respect to the unit direction considered as the measurment. Since the vector of the measured direction is initially unitary, the length of the bias vector introduced can be considered as $\tan\theta_{small} \approx \theta_{small}$, where θ_{small} represents the angle between real measurment and misaligned measurment. The θ_{small} selected is ...
- In the Simulink environment the white noise has to be defined through the power spectral density. This was selected as $N_p = \sigma^2 T_s$, where $sigma^2$ represents the variance as the standard deviation squared, while T_s is the sampling time of the sensor. It was decided to consider as standard deviation the value of 1 deg (that is the accuracy from Table 2)

7.2. Magnetometer

Due to the LEO orbit and seen that from subsection 6.5 the magnetic field was considered as one of the main disturbances, it was thought that a magnetometer could have been a sensor to implement on-board the satellite. This kind of sensor are in general less accurate than optical sensor as sun sensor or star sensor, but since the magnetic field of LEO orbit is effectively enough strong, the sensor can provide always a measurment. Also, having a magnetorquer assigned as mandatory, the coupling of this actuator with a magnetometer can be exploited during the de-tumbling manuever since a direct dipole command is produced by the so-called *B-dot Control*, extensively discussed in section (...)
The fluxgate magnetometer typology is used, where for each body axis, two ferromagnetic cores are used parallel to the specific axis. The primary coil saturates the two bars alternatively in opposite direction, so that the secondary output theoretically can read a null induced voltage output produced by the time-varying flux. When external field is present, the symmetry of the alternate saturation is broken so that a shift on the magnetic flux of the secondary coil is produced. This net flux can be read by the time-history of a voltmeter on the secondary coil, since the spacing of the measured output voltage depends on the external magnetic field value.
Since magnetometer are usually characterized by low accuracy values, we searched for a high-accuracy and low-noise typology. The research of a suitable sensor opted for *MM200* furnished by *AAC ClydeSpace*. The following performance paramters characterize the sensor:

$N.S.D\,[nT/\sqrt{Hz}]$	$Frequency\,[Hz]$
1.18	< 500

Table 3: Real data for Magnetometer Sensor

For the Simulink model, the same approach of the Horizon sensor in subsection 7.1 has been used. In particular, the magnetic fiel vector from the block of subsection 6.1 has been trasnformed into the $\mathcal{B}$ reference frame through the attitude matrix from the true kinematics block section 5. This is the input vector that has to be sampled with a frequency specified by Table 3. For this case a range of frequencies can be chosen: we used the same frequency of the horizon sensor from Table 2 since it respects the constraint given by the magnetometer requirments.
Then the measurments errors have to be added, a first misalignment error modeled in the same way of the horizon sensor in subsection 7.1. For this case the perpendicular vector has been scaled by a factor of (...). The accuracy error,

induced by the noise, has been modeled through a band-limited white noise added on each component. The value of the PSD is the square of the NSD presented in Table 3.

8. Attitude determination

The problem of estimating the attitude matrix from the available measurements is central to spacecraft control. To determine the attitude of the spacecraft, the sensor models introduced earlier were used. The method used to determine the attitude is the SVD method, which has been developed whitin the framework of Wahba's problem. The latter consists in finding the orthogonal matrix which minimizes the weighted cost function

$$J(A) = \frac{1}{2}\sum_{i=1}^{N} \alpha_i \|s_i - A_{BN} v_i\|^2$$

in which $\{s_i\}$ is a set of the N measured unit vectors in body frame and $\{v_i\}$ the corresponding set of unitt vectors in the inertial frame, computed using the on-board models. The set of weights $\{\alpha_i\}$ was chosen based on the relative accuracy of each sensor. It was assumed that the weight vector $\underline{\alpha}$ is normalized to 1, i.e. $\sum_{i=1}^{N} \alpha_i = 1$. This method needs at least two available measurements, so it works also in the case that the Earth is outside the FOV of the horizon sensor.
Since A is a orthogonal matrix and s_i and v_i are unit vectors, with some simple algebraic passages, the expression of J can be rewritten as:

$$J(A) = 1 - \sum_{i=1}^{N} \alpha_i (s_i^T A_{BN} v_i)$$

. The optimal solution minimizes J, therefore maximizes

$$\tilde{J}(A) = \sum_{i=1}^{N} \alpha_i (s_i^T A_{BN} v_i) = Tr(A_{BN} B^T)$$

where Tr is the trace operator and $B = \sum_{i=1}^{N} \alpha_i s_i v_i^T$.
Since a direct solution is computationally expensive, a single value decomposition technique is used. The matrix B can be decomposed as

$$B = USV^T = U diag([s_1 \;\; s_2 \;\; s_3])V^T$$

U and V are orthogonal matrices, representing the matrices of eigenvectors of BB^T and $B^T B$ respectively, S is the diagonal matrix containing the square roots of the eigenvalues of $B^T B$. We can define the matrices

$$U_+ = U diag([1 \;\; 1 \;\; det(U)]) \quad and \quad V_+ = V diag([1 \;\; 1 \;\; det(V)])$$

Then

$$B = U_+ S' V_+^T = B = U_+ diag([s_1 \;\; s_2 \;\; s_3'])V_+^T$$

where

$$s_3' = s_3 \det(U)\det(V)$$

Now it can be defined the matrix W and its representation in terms of Euler axis/angle:

$$W = U_+^T A V_+ = cos\theta I_3 - sin\theta[\vec{e}\times] + (1 - cos\theta)\vec{e}\vec{e}^T$$

$$Tr(AB^T) = Tr(WS') = \vec{e}^T S' \vec{e} + cos\theta(TrS' - \vec{e}^T S' \vec{e})$$

The trace is maximized for $\theta = 0$, which gives $W = I_3$ and thus the optimal attitude matrix is

$$A = U_+ V_+^T = U diag([1 \;\; 1 \;\; det(U) \cdot det(V)])V^T$$

9. Control logic

The control logic of the satellite is implemented on the computer that handle all the on-board calculations. In particular, all the data from the in-FOV sensors has to be gathered. Then, based on the mission phase, the necessary control has to be calculated and a command has to be sent to the system of actuators. The necessary control calculation is discussed in this section. Clearly, every phase of the mission is somehow different, this could be due to the mission requirments (i.e. detumble or pointing) or to the physical equations that describe the problem (linear or non-linear). Also, when a phase of the mission has to be analyzed and a control applied to it, all the possibilities and limitations coming from sensors and actuators has to be evaluated. As a consequence, the design of a control

logic is strictly related to the implementation of the actuators in the system, since even though a perfect control $\boldsymbol{u}$ can be designed by placing the fastest poles (in the linear case), then the actuator system will be highly penalized by not being able to perform that torque. As a consequence, it is important to bear in mind that when designing the control logic, always keep in consideration the actuators that will be used.
In the case under analysis, the magnetorquer actuators posses some useful and powerful proprerties, in particular when they are coupled with a magnetometer, the theory tells that the de-tumbling phase can be easily implemented [5]. On the other side, the control for a direction pointing (i.e. Nadir), in the case of magnetorquer is more difficult due to the unpleasent underactuated property of these magnetic systems. Infact, considering the equation of the actuator for the magnetorquer, and implementing that into the system equations, would result into a istantanteously uncontrollable system as cited in [6]. Nevertheless, by following the steps presented in [6], a fully magnetic actuated control can be reached but not without some effort and also drawbacks. In order not to complicate the next discussion, it was choosen the take into consideration also reaction wheels as a secondary actuator system.
In the next sub-sections the logic implemented in the Simulink environment will be presented, then all the more detailed actuator's cosniderations will be clarified.

9.1. De-tumbling phase: the B-dot control

The De-tumbling phase is performed immediately after the release of the spacecraft by the launcher, at this moment the angular velocities are random and depends on the launcher motion, also the attitude is initally unknown. In order to make the satellite ready to enter in the operational regime, so that it can start the pointing of the sensor's targets and the payload, the spacecraft must be de-tumbled. This means to create a control that decelerate the rotational velocities and fetch them to arbitrarly small values.
A frequently adopted option on magnetic-actuated satellites is to implement the so-called *B-dot control*, this method allows to exploit magnetic measurments to produce a direct magnetic dipole command to the magnetorquer which at the end leads to arbitrarly small values of ω. The increasing interest on this kind of control law is due to the fact that magnetorquers posses very intersting propreties, such as [5]:

- absence of catastrophic failure modes (an example of this would be the RW actuators which were characterized by catastrophic failure due to electrostatic charge on the bearing);
- reliable architecture which leads to unlimited operational life;
- the possibility to smoothly modulate the control torque, without inducing coupling with flexible modes (when bang-bang techniques are not adopted);
- significant savings in terms of weight and complexity since no moving parts are present.

Instead, the major drawback of this kind of system is surely the underactuated property. In general the magnetorquer cannot provide an arbitrarly oriented control torque due to the physical law that rules this device.

$$\boldsymbol{M_c} = \boldsymbol{D} \times \boldsymbol{B}_B \tag{4}$$

Clearly, it doesn't exist a $\boldsymbol{D}$ that satisfies the above equation if $\boldsymbol{M_c}$ and $\boldsymbol{B}$ are parallel. This implies to have, in general, a system that is not controllable at every istant, but it is in an averaged-sense. This implies a major difficulty in implementing a solely magnetic-actuated microsatellite. Avanzini et al. [5] demonstrate that asympotitc stability can be obtained through a law of this kind (using only magnetorquer and a magnetometer):

$$\boldsymbol{D} = -\frac{k_\omega}{||\boldsymbol{B}_B||}\dot{\hat{\boldsymbol{B}}}_{\boldsymbol{B}} \tag{5}$$

The idea of this kind of command is that the variation in magnetic field $\boldsymbol{B}$ in the $\mathcal{B}$ frame can be written as:

$$\dot{\boldsymbol{B}}_B = \frac{d\left(\boldsymbol{A}_{B,N}\boldsymbol{B}_N\right)}{dt} = \dot{\boldsymbol{A}}_{B,N}\boldsymbol{B}_N + \boldsymbol{A}_{B,N}\dot{\boldsymbol{B}}_N \approx \dot{\boldsymbol{A}}_{B,N}\boldsymbol{B}_N = -[\omega\times]\boldsymbol{A}_{B,N}\boldsymbol{B}_N = -[\omega\times]\boldsymbol{B}_B \tag{6}$$

The approximation symbol is due to the fact that when $\omega >> 1$, the variation of the magnetic field vector in $\mathcal{B}$ frame is mainly due to the rotation of the frame and less due to the changing of $\boldsymbol{b}_N$ (that is caused by the evolution in he orbital position and other slow variations due to geomagnetic field). With the above equation it has been demonstrated that $\boldsymbol{\omega}$ and $\dot{\boldsymbol{B}}$ are strictly related, so making the control law proportional to $\dot{\boldsymbol{B}}$ would be similar to make it proportional to $\boldsymbol{\omega}$ (like the 'standard' de-tumbling law). This mathematical considerations imply that for a detumbling law, it could be sufficient to have a magnetometer and a magnetorquer without a direct measurment of the angular velocity obtained by a gyro. Another positive consequence of having a proportional law that produces directly a magnetic dipole $\boldsymbol{D}$, is that the command is directly make as an input of the actuator (without inverting any actuator law). It is important to underline that this kind of law would work at his best when angular velocity is high enough to make the assumption of Equation 6 true. In theory the acutated torque is:

$$\boldsymbol{M_c} = -\frac{k_\omega}{||\boldsymbol{B}_B||}\dot{\hat{\boldsymbol{B}}}_{\boldsymbol{B}} \times \boldsymbol{B_B} \tag{7}$$

also notice that when $\omega >> 1$ Equation 6 is more and more true, and so $\boldsymbol{B}_B$ and $\dot{\hat{\boldsymbol{B}}}_B$ are perpendicular, resulting in the maximum actuable control torque.
Regarding the control law Equation 5, it has to be seen that the vector derived is not the derivative of the magnetic field vector, but it is the derivative of the unit vector of the direction of the magnetic field. Also, notice that all the vector in the above relationship are in the $\mathcal{B}$ frame since the magnetic field vector $\boldsymbol{B}$ comes from the magnetometer measurment.
In the context of the simulation environment on Simulink, the formulation choosen for the b-dot control comes from [5] of Avanzini et Al. Some precaution has to be taken when implementing the law, since the numerical derivative of a mesaured (hence noisy) signal has to be performed. This inconvinence can be overcome by using a low-pass filter [4]. In order to make some sense out of the calculation, a discrete low-pass Butterworth filter of the 1st order has been used just after the discrete derivative block. Setting the cut-off frequency on 0.06 rad/s the signal is pretty clean and the results of simulation are coherent

9.2. Slew and Nadir phase

10. Actuators

10.1. Reaction Wheels

Reaction wheels are one of the primary attitude control actuators for control in spacecraft as they can give precise pointing and be controlled through feedback actively. They are based on acceleration and deceleration of spinning rotors. If the nominal condition is with a null angular velocity then that is a defining characteristic for reaction wheels as actuator.

Now, the equations for a dual spin satellite with no external torques applied are:

$$I_r \dot{\omega}_r = M_r$$

$$I_z \dot{\omega}_z = -I_r \dot{\omega}_r$$

The torque M_r is generated by an electric motor, which follows a characteristic performance curve. The general problem of control with reaction wheels can be modelled through the adequate set of Euler equations which contains the effects of the n actuators in the expression of the angular momentum:

$$\mathbf{h} = I\boldsymbol{\omega} + \Delta\mathbf{h}_r$$

To simplify the solution of the control problem, considering the dynamics following the previous expression, we group the equation terms for determining the control torque required and the the effective control command for the reaction wheels:

$$I\dot{\boldsymbol{\omega}} + \boldsymbol{\omega} \times I\boldsymbol{\omega} + \boldsymbol{\omega} \times \Delta\mathbf{h}_r + \Delta\dot{\mathbf{h}}_r = \mathbf{T}$$
$$\mathbf{M}_c = -\boldsymbol{\omega} \times \Delta\mathbf{h}_r - \Delta\dot{\mathbf{h}}_r$$
$$I_r\dot{\boldsymbol{\omega}} = \mathbf{M}_r$$

The equation for the evaluation of the control law, hence, stands as:

$$I\dot{\boldsymbol{\omega}} + \boldsymbol{\omega} \times I\boldsymbol{\omega} = \mathbf{T} + \mathbf{M}_c$$

Once $\mathbf{M}_c$ is calculated using any suitable linear control design technique, $\mathbf{M}_r$ can be evaluated using the following procedure:

$$\Delta\mathbf{h}_r = -\mathbf{M}_c - \boldsymbol{\omega} \times \Delta\mathbf{h}_r$$
$$\dot{\mathbf{h}}_r = -\mathbf{A}^*(\mathbf{M}_c + \boldsymbol{\omega} \times \Delta\mathbf{h}_r)$$

Here $\mathbf{A}^*$ is the pseudo inverse matrix of $\mathbf{A}$ for the general case.

Bibliography

[1] Georce C. Marshall Space Flight Center. *Saturn V Flight Manual SA-507*. National Aeronautics and Space Administration, 10 1969.

[2] Howard D. Curtis. *Orbital Mechanics for Engineering Students*. Elsevier, 2014.

[3] ESA. Types of orbits. Website, 2020. Site: `https://www.esa.int/Enabling_Support/Space_Transportation/Types_of_orbits`.

[4] John l. Crassidis F. Landis Markley. *Fundamentals of Spacecraft Attitude Determination and Control*. Springer, 2014.

[5] Giulio Avanzini, Fabrizio Giulietti. Magnetic Detumbling of a Rigid Spacecraft. *Journal of Guidance, Control and Dynamics*, 35(4):1326–1333, 8 2012.

[6] M. Lovera, A. Astolfi. Spacecraft attitude control using magnetic actuators. *Elsevier*, 40(4):1405–1414, 2 2004.